

## Dehydration of Glycerin to Acrolein Over $H_3PW_{12}O_{40}$ Catalyst Supported on Mesoporous Titania

Tae Hun Kang<sup>1</sup>, Jung Ho Choi<sup>1</sup>, Min Yeong Gim<sup>1</sup>, Jun Seon Choi<sup>2</sup>, Wangrae Joe<sup>2</sup>, and In Kyu Song<sup>1,\*</sup>

<sup>1</sup>School of Chemical and Biological Engineering, Institute of Chemical Processes, Seoul National University, Shinlim-dong, Kwanak-ku, Seoul 151-744, South Korea

<sup>2</sup>LG Chem. Ltd., Moonji-dong, Yuseong-Gu, Daejeon 305-380, South Korea

$H_3PW_{12}O_{40}$  catalysts supported on mesoporous titania ( $XH_3PW_{12}O_{40}/MT$  ( $X = 5, 10, 15, 20, 25,$  and  $30$ )) were prepared with a variation of  $H_3PW_{12}O_{40}$  content ( $X$ , wt%), and they were applied to the dehydration of glycerin to acrolein. The prepared catalysts were characterized by FT-IR spectroscopy, X-ray diffraction,  $N_2$  adsorption–desorption, and pyridine-adsorbed *in-situ* FT-IR spectroscopy analyses. The effect of  $H_3PW_{12}O_{40}$  content on the physicochemical properties and catalytic activities of  $XH_3PW_{12}O_{40}/MT$  catalysts was investigated. It was found that surface area and pore volume of  $XH_3PW_{12}O_{40}/MT$  catalysts decreased with increasing  $H_3PW_{12}O_{40}$  content. Brønsted acidity of  $XH_3PW_{12}O_{40}/MT$  catalysts showed a volcano-shaped trend with respect to  $H_3PW_{12}O_{40}$  content. The catalytic performance of  $XH_3PW_{12}O_{40}/MT$  catalysts was closely related to the Brønsted acidity of the catalysts. It was revealed that yield for acrolein over  $XH_3PW_{12}O_{40}/MT$  catalysts increased with increasing Brønsted acidity of the catalysts. Among the catalysts tested,  $20H_3PW_{12}O_{40}/MT$  catalyst with the largest Brønsted acidity showed the highest yield for acrolein.

**Keywords:** Heteropolyacid, Mesoporous Titania, Dehydration of Glycerin, Acrolein, Brønsted Acidity.

### 1. INTRODUCTION

Due to fossil fuel depletion and new energy policy, biomass has attracted much attention as a clean energy resource.<sup>1–3</sup> In the production of biodiesel from biomass resource, a considerable amount of glycerin is formed as a by-product (10% by weight).<sup>1,2</sup> Therefore, a number of researches have been conducted to find new applications to convert low-value glycerin feedstock into value-added chemicals.<sup>4–6</sup> Among the catalytic processes for glycerin conversion, catalytic dehydration of glycerin to acrolein is one of the most promising research areas due to versatile applicability of acrolein as a chemical intermediate for the synthesis of acrylic acid, methionine, and super-absorbent polymers.<sup>7,8</sup> Acrolein has been conventionally produced by partial oxidation process of petroleum-based propylene over multi-component metal oxide catalysts.<sup>9</sup> However, the catalytic dehydration of glycerin to acrolein has recently become a promising route for acrolein production due to economical and environmental advantages in

comparison with the petroleum-based process.<sup>1,2</sup> Several solid acid catalysts including zeolites,<sup>10</sup> metal oxides,<sup>11</sup> and phosphates<sup>12</sup> have been investigated as catalysts for gas-phase dehydration of glycerin. However, a previous work showed that the acid-catalyzed dehydration of glycerin suffered from catalyst deactivation and low catalytic activity due to coke formation and considerable activation energy, respectively.<sup>7</sup>

It has been reported that Brønsted acid strength of heteropolyacids (HPAs) is stronger than that of conventional solid acid.<sup>13,14</sup> For this reason, HPAs have been utilized as benign solid acid catalysts in several acid-catalyzed reactions. However, one of the disadvantages of HPA catalysts is their low surface area ( $<10$  m<sup>2</sup>/g), leading to fast catalyst deactivation during a long-time reaction. To overcome this problem, HPAs supported on mesoporous materials with high surface area such as silica, alumina, and activated carbon have been investigated as catalysts for acid-catalyzed reactions. Among them, titania has been widely used as a support because of its outstanding textural properties.<sup>15,16</sup>

\* Author to whom correspondence should be addressed.

In this work, a series of  $\text{H}_3\text{PW}_{12}\text{O}_{40}$  catalysts supported on mesoporous titania ( $\text{XH}_3\text{PW}_{12}\text{O}_{40}/\text{MT}$  ( $X = 5, 10, 15, 20, 25,$  and  $30$ )) were prepared with a variation of  $\text{H}_3\text{PW}_{12}\text{O}_{40}$  content ( $X$ , wt%) to investigate the effect of  $\text{H}_3\text{PW}_{12}\text{O}_{40}$  content on the physicochemical properties and catalytic activities in the dehydration of glycerin to acrolein. The prepared catalysts were characterized by ICP-AES, FT-IR, XRD, and nitrogen adsorption–desorption analyses. Pyridine-adsorbed *in-situ* FT-IR spectroscopy analyses were also conducted to examine the acid properties of  $\text{XH}_3\text{PW}_{12}\text{O}_{40}/\text{MT}$  catalysts. A correlation between acid properties and catalytic activities in the dehydration of glycerin to acrolein was then established and discussed.

## 2. EXPERIMENTAL DETAILS

### 2.1. Preparation of Catalysts

Mesoporous titania support was prepared by a sol–gel method according to the procedures in the literature.<sup>17</sup> Titanium butoxide (TB, Sigma-Aldrich) was dissolved in absolute ethanol, and it was stirred for 30 min to obtain a homogeneous solution. Hydrochloric acid (HCl, Sigma-Aldrich) was added into the TB solution at a constant rate for 2 h to form an alcogel. The alcogel was further aged at room temperature for 48 h and it was dried at 100 °C for 24 h. The resulting yellow solid was finally calcined at 400 °C for 5 h. The prepared mesoporous titania support was denoted as MT.  $\text{XH}_3\text{PW}_{12}\text{O}_{40}/\text{MT}$  catalysts with different  $\text{H}_3\text{PW}_{12}\text{O}_{40}$  content ( $X$ , wt%) were then prepared by an incipient wetness impregnation method. For this, a known amount of tungstophosphoric acid ( $\text{H}_3\text{PW}_{12}\text{O}_{40}$ ) was dissolved in distilled water, and pH of the solution was adjusted to be 1.0 using hydrochloric acid. The solution containing  $\text{H}_3\text{PW}_{12}\text{O}_{40}$  was then added into MT support. The mixture was stirred and evaporated at 80 °C. The impregnated catalyst was dried at 100 °C for 12 h, and it was calcined at 300 °C for 5 h. The prepared catalysts were denoted as  $\text{XH}_3\text{PW}_{12}\text{O}_{40}/\text{MT}$  ( $X = 5, 10, 15, 20, 25,$  and  $30$ ), where  $X$  represented the weight percentage of  $\text{H}_3\text{PW}_{12}\text{O}_{40}$ .

### 2.2. Characterization of Catalysts

$\text{H}_3\text{PW}_{12}\text{O}_{40}$  contents in the  $\text{XH}_3\text{PW}_{12}\text{O}_{40}/\text{MT}$  catalysts were determined by inductively coupled plasma-atomic emission spectrometry (ICP-AES) analyses (Shimadzu, ICP-1000IV). Infrared spectra of the catalysts were obtained with a Fourier transform infrared (FT-IR) spectrometer (Thermo Scientific, Nicolet 6700). X-ray diffraction (XRD) patterns of the catalysts were obtained by XRD measurements (Rigaku, D-MAX2500-PC) using  $\text{Cu-K}\alpha$  radiation operated at 50 kV and 100 mA. Nitrogen adsorption–desorption experiments (BEL Japan, BELSORP-mini II) were conducted to examine the textural properties of the catalysts. Pore size distributions

of the catalysts were determined by BJH (Barret-Joyner-Hallender) method.

Acid properties of  $\text{XH}_3\text{PW}_{12}\text{O}_{40}/\text{MT}$  catalysts were determined by pyridine-adsorbed *in-situ* FT-IR spectroscopy measurements. Each catalyst (0.04 g) was pressed into a pellet with a radius of 0.65 cm. The pellet was preheated at 200 °C for 1 h with a stream of He (40 ml/min) in a tubular quartz cell. After cooling the pellet to 50 °C, pyridine vapor (5 ml) was pulsed into the reactor with a stream of He (40 ml/min) until the acid sites were saturated with pyridine. The reactor was evacuated at 50 °C for 1 h. IR spectra were then recorded at 50 °C within the spectral range of 1600–1400  $\text{cm}^{-1}$ .

### 2.3. Gas-Phase Dehydration of Glycerin

Gas-phase dehydration of glycerin was carried out at 275 °C under atmospheric pressure in a continuous flow fixed-bed reactor. The tubular pyrex reactor was packed with a catalyst (0.1 g), and it was preheated with a stream of nitrogen carrier gas (30 ml/min) at 275 °C for 0.5 h to achieve steady-state operation. Glycerin feed (7 mol% aqueous solution, 1.0 mmol/h) was sufficiently vaporized by passing through a pre-heating zone, and it was continuously fed into the reactor together with nitrogen carrier (30 ml/min). The reaction was carried out at 275 °C for 5 h. The reaction products were analyzed using a gas chromatograph equipped with a flame ionization detector (Younglin, YL6100 GC) and a capillary column (Agilent, DB-5MS, 60 m  $\times$  0.32 mm). 1,4-Dioxane (Samchun Chem.) was used as an internal standard for quantitative calculation. Conversion of glycerin, selectivity for product, and yield for product were calculated according to the following equations.

Conversion of glycerin (%)

$$= \frac{\text{mole of glycerin inlet} - \text{mole of glycerin outlet}}{\text{mole of glycerin inlet}} \times 100 \quad (1)$$

Selectivity for product (%)

$$= \frac{\text{mole of product outlet}}{\text{mole of glycerin inlet} - \text{mole of glycerin outlet}} \times 100 \quad (2)$$

$$\text{Yield for product (\%)} = \frac{\text{mole of product outlet}}{\text{mole of glycerin inlet}} \times 100 \quad (3)$$

## 3. RESULTS AND DISCUSSION

### 3.1. Characterization of $\text{XH}_3\text{PW}_{12}\text{O}_{40}/\text{MT}$ Catalysts

Figure 1 shows the FT-IR spectra of MT,  $\text{H}_3\text{PW}_{12}\text{O}_{40}$ , and  $\text{XH}_3\text{PW}_{12}\text{O}_{40}/\text{MT}$  ( $X = 5, 10, 15, 20, 25,$  and  $30$ ) catalysts. IR spectrum of MT was well consistent with the result in the previous literature.<sup>18</sup>  $\text{H}_3\text{PW}_{12}\text{O}_{40}$  exhibited four characteristic IR bands appearing at 1080  $\text{cm}^{-1}$

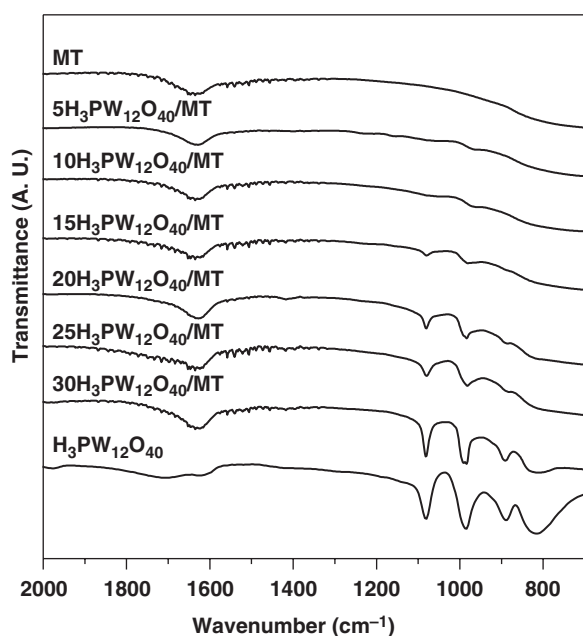
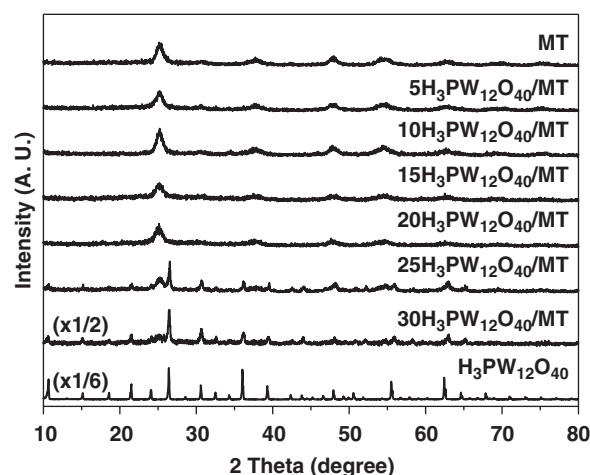


**Figure 1.** FT-IR spectra of MT,  $\text{H}_3\text{PW}_{12}\text{O}_{40}$ , and  $\text{XH}_3\text{PW}_{12}\text{O}_{40}/\text{MT}$  ( $X = 5, 10, 15, 20, 25,$  and  $30$ ) catalysts.

(P–O band),  $983\text{ cm}^{-1}$  (W=O band),  $890\text{ cm}^{-1}$  (W–O<sub>c</sub>–W band), and  $812\text{ cm}^{-1}$  (W–O<sub>e</sub>–W band), corresponding to the primary structure of  $\text{H}_3\text{PW}_{12}\text{O}_{40}$ .<sup>19</sup> These four characteristic IR bands were not clearly observed in the  $5\text{H}_3\text{PW}_{12}\text{O}_{40}/\text{MT}$  and  $10\text{H}_3\text{PW}_{12}\text{O}_{40}/\text{MT}$  catalysts because of low  $\text{H}_3\text{PW}_{12}\text{O}_{40}$  content. However, the four characteristic IR bands were observed in the  $15\text{H}_3\text{PW}_{12}\text{O}_{40}/\text{MT}$ ,  $20\text{H}_3\text{PW}_{12}\text{O}_{40}/\text{MT}$ ,  $25\text{H}_3\text{PW}_{12}\text{O}_{40}/\text{MT}$ , and  $30\text{H}_3\text{PW}_{12}\text{O}_{40}/\text{MT}$  catalysts. Moreover, peak intensities of characteristic IR bands corresponding to  $\text{H}_3\text{PW}_{12}\text{O}_{40}$  increased with increasing  $\text{H}_3\text{PW}_{12}\text{O}_{40}$  content. This result indicates that the primary structure of  $\text{H}_3\text{PW}_{12}\text{O}_{40}$  was still maintained even after the impregnation of  $\text{H}_3\text{PW}_{12}\text{O}_{40}$  on MT.

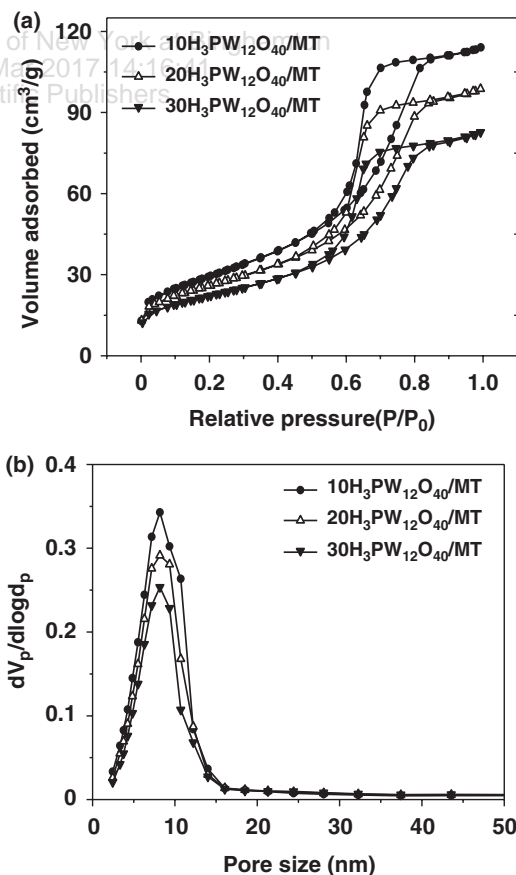
Figure 2 shows the XRD patterns of MT,  $\text{H}_3\text{PW}_{12}\text{O}_{40}$ , and  $\text{XH}_3\text{PW}_{12}\text{O}_{40}/\text{MT}$  ( $X = 5, 10, 15, 20, 25,$  and  $30$ ) catalysts. The diffraction patterns of MT indicates that MT retained an anatase structure.<sup>20</sup> It was observed that  $\text{XH}_3\text{PW}_{12}\text{O}_{40}/\text{MT}$  catalysts with low  $\text{H}_3\text{PW}_{12}\text{O}_{40}$  loading ( $X = 5, 10, 15,$  and  $20$ ) did not show characteristic diffraction peaks for  $\text{H}_3\text{PW}_{12}\text{O}_{40}$ , indicating that  $\text{H}_3\text{PW}_{12}\text{O}_{40}$  was finely dispersed on the support. On the other hand, XRD peaks for  $\text{H}_3\text{PW}_{12}\text{O}_{40}$  were observed in the  $\text{XH}_3\text{PW}_{12}\text{O}_{40}/\text{MT}$  catalysts with high  $\text{H}_3\text{PW}_{12}\text{O}_{40}$  loading ( $X = 25$  and  $30$ ) due to aggregation of  $\text{H}_3\text{PW}_{12}\text{O}_{40}$ . Furthermore, intensity of XRD peaks for  $\text{H}_3\text{PW}_{12}\text{O}_{40}$  increased with increasing  $\text{H}_3\text{PW}_{12}\text{O}_{40}$  content, indicating that aggregation of  $\text{H}_3\text{PW}_{12}\text{O}_{40}$  was dominant with increasing  $\text{H}_3\text{PW}_{12}\text{O}_{40}$  content.

Figure 3 shows the nitrogen adsorption–desorption isotherms and pore size distributions of  $\text{XH}_3\text{PW}_{12}\text{O}_{40}/\text{MT}$  ( $X = 10, 20,$  and  $30$ ) catalysts.  $\text{XH}_3\text{PW}_{12}\text{O}_{40}/\text{MT}$  catalysts



**Figure 2.** XRD patterns of MT,  $\text{H}_3\text{PW}_{12}\text{O}_{40}$ , and  $\text{XH}_3\text{PW}_{12}\text{O}_{40}/\text{MT}$  ( $X = 5, 10, 15, 20, 25,$  and  $30$ ) catalysts.

exhibited type-IV isotherm with H2 hysteresis loop. Nitrogen adsorption–desorption isotherms and pore size distributions of  $\text{XH}_3\text{PW}_{12}\text{O}_{40}/\text{MT}$  catalysts were similar to those of MT support (not shown here), indicating that pore structure of support was maintained even after the impregnation of  $\text{H}_3\text{PW}_{12}\text{O}_{40}$  on the support. Surface area, pore



**Figure 3.** (a) Nitrogen adsorption–desorption isotherms and (b) pore size distributions of  $\text{XH}_3\text{PW}_{12}\text{O}_{40}/\text{MT}$  ( $X = 10, 20,$  and  $30$ ) catalysts.

**Table I.** Physicochemical properties of  $\text{XH}_3\text{PW}_{12}\text{O}_{40}/\text{MT}$  catalysts.

Catalyst	$\text{H}_3\text{PW}_{12}\text{O}_{40}$ content (wt%) <sup>a</sup>	Surface area ( $\text{m}^2/\text{g}$ ) <sup>b</sup>	Pore volume ( $\text{cm}^3/\text{g}$ ) <sup>c</sup>	Average pore diameter (nm) <sup>d</sup>	Brønsted acidity (mmol-pyridine/g-cat.)	Lewis acidity (mmol-pyridine/g-cat.)
$5\text{H}_3\text{PW}_{12}\text{O}_{40}/\text{MT}$	4.8	120.3	0.187	8.3	0.346	0.734
$10\text{H}_3\text{PW}_{12}\text{O}_{40}/\text{MT}$	9.4	105.8	0.172	8.2	0.512	0.692
$15\text{H}_3\text{PW}_{12}\text{O}_{40}/\text{MT}$	14.5	97.2	0.159	8.1	0.569	0.673
$20\text{H}_3\text{PW}_{12}\text{O}_{40}/\text{MT}$	19.1	91.6	0.148	8.2	0.762	0.584
$25\text{H}_3\text{PW}_{12}\text{O}_{40}/\text{MT}$	23.8	84.3	0.131	8.2	0.726	0.541
$30\text{H}_3\text{PW}_{12}\text{O}_{40}/\text{MT}$	28.6	78.0	0.123	8.2	0.665	0.503

Notes: <sup>a</sup>Determined by ICP-AES measurement; <sup>b</sup>Calculated by BET equation; <sup>c</sup>BJH desorption pore volume; <sup>d</sup>BJH desorption average pore diameter.

volume, and average pore diameter of  $\text{H}_3\text{PW}_{12}\text{O}_{40}/\text{MT}$  catalysts are summarized in Table I. It was found that surface area and pore volume of  $\text{XH}_3\text{PW}_{12}\text{O}_{40}/\text{MT}$  catalysts decreased with increasing  $\text{H}_3\text{PW}_{12}\text{O}_{40}$  content. However, average pore diameter of  $\text{XH}_3\text{PW}_{12}\text{O}_{40}/\text{MT}$  catalysts was almost the same. It was also observed that  $\text{H}_3\text{PW}_{12}\text{O}_{40}$  contents in the  $\text{XH}_3\text{PW}_{12}\text{O}_{40}/\text{MT}$  ( $X = 5, 10, 15, 20, 25,$  and  $30$ ) catalysts were well consistent with the designed values, indicating that all the catalysts were successfully prepared in this work.

### 3.2. Acid Properties of $\text{XH}_3\text{PW}_{12}\text{O}_{40}/\text{MT}$ Catalysts

In order to investigate the acid properties of  $\text{XH}_3\text{PW}_{12}\text{O}_{40}/\text{MT}$  ( $X = 5, 10, 15, 20, 25,$  and  $30$ ) catalysts, pyridine-adsorbed *in-situ* FT-IR spectroscopy measurements were carried out. Figure 4 shows the pyridine-adsorbed *in-situ* FT-IR spectra of  $\text{XH}_3\text{PW}_{12}\text{O}_{40}/\text{MT}$  catalysts. IR bands were assigned according to the previous study.<sup>21</sup> All the  $\text{XH}_3\text{PW}_{12}\text{O}_{40}/\text{MT}$  catalysts exhibited IR bands due to Lewis acid-bound pyridine ( $1450$  and  $1490\text{ cm}^{-1}$ ) and Brønsted acid-bound pyridinium ion ( $1490$  and  $1545\text{ cm}^{-1}$ ). Brønsted acidity and Lewis acidity of  $\text{XH}_3\text{PW}_{12}\text{O}_{40}/\text{MT}$  catalysts were quantitatively measured according to the method in the literature<sup>22</sup> as summarized in Table I.

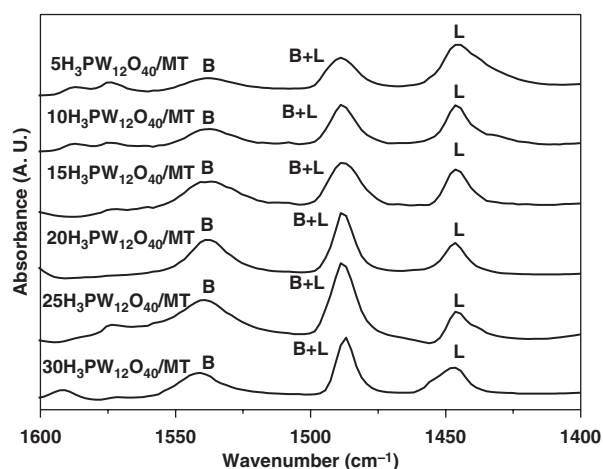
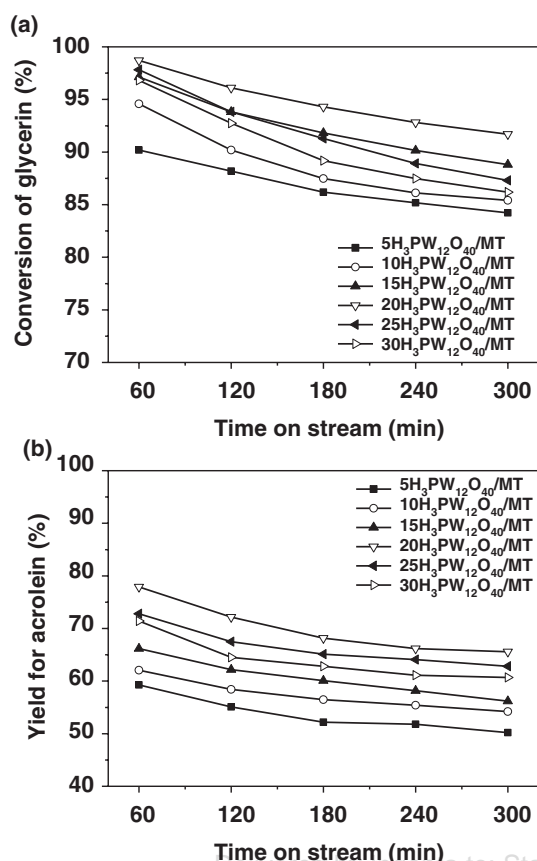


**Figure 4.** Pyridine-adsorbed *in-situ* FT-IR spectra of  $\text{XH}_3\text{PW}_{12}\text{O}_{40}/\text{MT}$  ( $X = 5, 10, 15, 20, 25,$  and  $30$ ) catalysts.

It was found that Brønsted acidity of the catalysts showed a volcano-shaped trend with respect to  $\text{H}_3\text{PW}_{12}\text{O}_{40}$  content. Among the catalysts tested,  $20\text{H}_3\text{PW}_{12}\text{O}_{40}/\text{MT}$  retained the largest Brønsted acidity. It has been reported in the previous literature<sup>23</sup> that acidity of  $\text{H}_3\text{PW}_{12}\text{O}_{40}$  impregnated on silica support did not increase in proportion to  $\text{H}_3\text{PW}_{12}\text{O}_{40}$  which possessed pure Brønsted acid sites. It has also been reported that acidity of impregnated catalysts with high  $\text{H}_3\text{PW}_{12}\text{O}_{40}$  content decreased, because  $\text{H}_3\text{PW}_{12}\text{O}_{40}$  agglomerates were caged in the pore walls and blocked the pores, leading to a decreased amount of  $\text{H}_3\text{PW}_{12}\text{O}_{40}$  exposed on the surface and leading to poor diffusion of reactant onto the acid sites.<sup>23, 24</sup> In this work, formation of  $\text{H}_3\text{PW}_{12}\text{O}_{40}$  aggregates was also observed in the  $\text{XH}_3\text{PW}_{12}\text{O}_{40}/\text{MT}$  catalysts with high  $\text{H}_3\text{PW}_{12}\text{O}_{40}$  loading. Therefore, it can be inferred that Brønsted acidity of  $\text{XH}_3\text{PW}_{12}\text{O}_{40}/\text{MT}$  catalysts exhibited a volcano-shaped trend with respect to  $\text{H}_3\text{PW}_{12}\text{O}_{40}$  content due to restricted exposure of  $\text{H}_3\text{PW}_{12}\text{O}_{40}$  and diffusional restraint of pyridine. Moreover, it was also found that Lewis acidity of the catalysts decreased with increasing  $\text{H}_3\text{PW}_{12}\text{O}_{40}$  content. It is believed that surface  $\text{Ti}^{4+}$  cations, which served as Lewis acid sites, were blocked by the impregnated  $\text{H}_3\text{PW}_{12}\text{O}_{40}$  species.

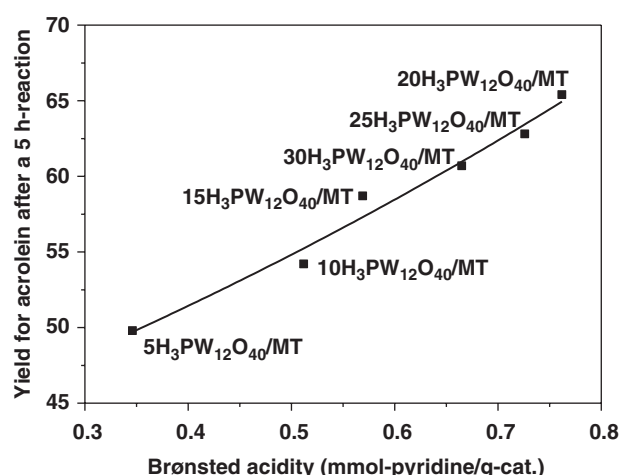
### 3.3. Catalytic Performance of $\text{XH}_3\text{PW}_{12}\text{O}_{40}/\text{MT}$ Catalysts

Figure 5 shows the conversion of glycerin and yield for acrolein over  $\text{XH}_3\text{PW}_{12}\text{O}_{40}/\text{MT}$  ( $X = 5, 10, 15, 20, 25,$  and  $30$ ) catalysts with time on stream in the dehydration of glycerin at  $275\text{ }^\circ\text{C}$ . Conversion of glycerin, selectivity for product, and yield for acrolein after a 5 h-reaction are summarized in Table II. According to the literature,<sup>10</sup> catalytic dehydration of glycerin follows consecutive reaction pathways. Acid catalyst initiates the formation of primary and secondary carbocations, and the secondary carbocation is more stable than primary carbocation due to the thermodynamic effect. Thus, acrolein formed through two-step dehydration via secondary carbocation was a main product, while hydroxyacetone formed from primary carbocation was a major by-product. Other compounds such as allyl alcohol, acetaldehyde, acetic acid, and acetone were produced as minor by-products in the dehydration of glycerin.<sup>7, 8</sup>



**Figure 5.** (a) Conversion of glycerin and (b) yield for acrolein over  $\text{XH}_3\text{PW}_{12}\text{O}_{40}/\text{MT}$  ( $X = 5, 10, 15, 20, 25,$  and  $30$ ) catalysts with time on stream in the dehydration of glycerin at  $275^\circ\text{C}$ .

It was observed that the catalytic performance of  $\text{XH}_3\text{PW}_{12}\text{O}_{40}/\text{MT}$  catalysts gradually decreased with time on stream during the 5 h-reaction. The spent  $\text{XH}_3\text{PW}_{12}\text{O}_{40}/\text{MT}$  catalysts were collected after the 5 h-reaction and investigated by CNHS analyses. The amount of carbon deposition in the spent  $\text{XH}_3\text{PW}_{12}\text{O}_{40}/\text{MT}$  catalysts determined by CHNS analyses is summarized in Table II. It is believed that carbonaceous materials formed during the dehydration reaction blocked the active sites of the catalysts, resulting in catalyst deactivation with time on



**Figure 6.** A correlation between yield for acrolein after a 5 h-reaction over  $\text{XH}_3\text{PW}_{12}\text{O}_{40}/\text{MT}$  ( $X = 5, 10, 15, 20, 25,$  and  $30$ ) catalysts and Brønsted acidity of the catalysts.

stream. Furthermore, the calculated carbon balance after the 5 h-reaction (Table II) was less than 100% due to carbon deposition derived from polymerization of acrolein and oligomerization of glycerin.<sup>25, 26</sup>

It was revealed that yield for acrolein increased in the order of  $5\text{H}_3\text{PW}_{12}\text{O}_{40}/\text{MT} < 10\text{H}_3\text{PW}_{12}\text{O}_{40}/\text{MT} < 15\text{H}_3\text{PW}_{12}\text{O}_{40}/\text{MT} < 30\text{H}_3\text{PW}_{12}\text{O}_{40}/\text{MT} < 25\text{H}_3\text{PW}_{12}\text{O}_{40}/\text{MT} < 20\text{H}_3\text{PW}_{12}\text{O}_{40}/\text{MT}$ . This trend of yield for acrolein over  $\text{XH}_3\text{PW}_{12}\text{O}_{40}/\text{MT}$  ( $X = 5, 10, 15, 20, 25,$  and  $30$ ) catalysts was closely related to the Brønsted acidity of the catalysts. Figure 6 shows the correlation between yield for acrolein after a 5 h-reaction over  $\text{XH}_3\text{PW}_{12}\text{O}_{40}/\text{MT}$  ( $X = 5, 10, 15, 20, 25,$  and  $30$ ) catalysts and Brønsted acidity of the catalysts. It is interesting to note that yield for acrolein increased with increasing Brønsted acidity of the catalysts, in good agreement with the previous works.<sup>27, 28</sup> In case of Brønsted acid sites, proton can be easily transferred to internal oxygen of glycerin due to the absence of steric hindrance. Therefore, Brønsted acid sites mainly protonate the internal oxygen of glycerin, leading to the formation of acrolein via secondary carbocation. However, interaction

**Table II.** Conversion of glycerin, selectivity for product, yield for acrolein, carbon balance, and amount of carbon deposition over  $\text{XH}_3\text{PW}_{12}\text{O}_{40}/\text{MT}$  catalysts after a 5 h-reaction.

Catalyst	Conversion of glycerin (%)	Selectivity for product (%)					Yield for acrolein (%)	Carbon balance (%)	Amount of carbon deposition (%)
		Acrolein	Hydroxy-acetone	Ally alcohol	Acetal-dehyde	Others <sup>a</sup>			
$5\text{H}_3\text{PW}_{12}\text{O}_{40}/\text{MT}$	83.4	59.7	8.3	2.5	1.6	19.3	49.8	91.4	3.7
$10\text{H}_3\text{PW}_{12}\text{O}_{40}/\text{MT}$	85.4	63.5	8.2	3.1	1.4	16.9	54.2	93.1	4.3
$15\text{H}_3\text{PW}_{12}\text{O}_{40}/\text{MT}$	88.7	66.1	7.4	3.4	1.9	16.6	58.7	95.4	4.5
$20\text{H}_3\text{PW}_{12}\text{O}_{40}/\text{MT}$	91.7	71.3	6.5	3.0	1.8	12.9	65.4	95.5	5.3
$25\text{H}_3\text{PW}_{12}\text{O}_{40}/\text{MT}$	87.3	71.9	5.8	2.6	2.3	11.6	62.8	94.2	5.0
$30\text{H}_3\text{PW}_{12}\text{O}_{40}/\text{MT}$	86.1	70.4	5.9	2.8	2.1	12.6	60.7	93.8	4.6

Note: <sup>a</sup>Others contain acetic acid, acetone, and several unidentified products.

of glycerin with Lewis acid sites can be affected by steric constraints due to the electronic structure of Lewis acid sites. For this reason, terminal oxygen of glycerin is more likely to interact with Lewis acid sites. As a result, hydroxyacetone is mainly produced on the Lewis acid sites via primary carbocation. Among the catalysts tested,  $20\text{H}_3\text{PW}_{12}\text{O}_{40}/\text{MT}$  catalyst with largest Brønsted acidity showed the highest yield for acrolein. Thus, Brønsted acidity of the catalysts played an important role in the catalytic dehydration of glycerin to acrolein.

#### 4. CONCLUSIONS

Gas-phase dehydration of glycerin to acrolein was carried out over  $\text{H}_3\text{PW}_{12}\text{O}_{40}$  catalysts supported on mesoporous titania ( $\text{XH}_3\text{PW}_{12}\text{O}_{40}/\text{MT}$ ) with different  $\text{H}_3\text{PW}_{12}\text{O}_{40}$  content ( $X$ , wt%). Yield for acrolein over  $\text{XH}_3\text{PW}_{12}\text{O}_{40}/\text{MT}$  catalysts showed a volcano-shaped trend with respect to  $\text{H}_3\text{PW}_{12}\text{O}_{40}$  content. Brønsted acidity of the catalysts determined from pyridine-adsorbed *in-situ* FT-IR spectroscopy also exhibited a volcano-shaped trend with respect to  $\text{H}_3\text{PW}_{12}\text{O}_{40}$  content. It was revealed that the catalytic performance of  $\text{XH}_3\text{PW}_{12}\text{O}_{40}/\text{MT}$  ( $X = 5, 10, 15, 20, 25$ , and  $30$ ) catalysts in the dehydration of glycerin was closely related to the Brønsted acidity of the catalysts. Yield for acrolein over  $\text{XH}_3\text{PW}_{12}\text{O}_{40}/\text{MT}$  ( $X = 5, 10, 15, 20, 25$ , and  $30$ ) catalysts increased with increasing Brønsted acidity of the catalysts. Among the catalysts tested,  $20\text{H}_3\text{PW}_{12}\text{O}_{40}/\text{MT}$  with the largest Brønsted acidity showed the highest yield for acrolein. In conclusion, Brønsted acidity of the catalysts served as a key factor determining the catalytic performance in the dehydration of glycerin to acrolein.

**Acknowledgments:** The authors wish to acknowledge the support from LG Chemical Corporation.

#### References and Notes

1. A. Srivastava and R. Prasad, *Renewable Sustainable Energy Rev.* 4, 113 (2000).
2. K.-W. Lee, J. X. Yu, J. H. Mei, L. Yan, Y.-W. Kim, and K.-W. Chung, *J. Ind. Eng. Chem.* 13, 799 (2007).
3. E. Garcia, M. Laca, E. Perez, A. Garrido, and J. Peinado, *Energy Fuels* 22, 4274 (2008).
4. A. M. Ruppert, J. D. Meeldijk, B. W. M. Kuipers, B. H. Ern , and B. M. Weckhuyzen, *Chem. Eur. J.* 14, 2016 (2008).
5. J. Chaminand, L. Djakovitch, P. Gallezot, P. Marion, C. Pinel, and C. Rosier, *Green Chem.* 6, 359 (2004).
6. G. P. da Silva, M. Mack, and J. Contiero, *Biotechnol. Adv.* 27, 30 (2009).
7. L. Liu, X. P. Ye, and J. J. Bozell, *ChemSusChem.* 5, 1162 (2012).
8. B. Katryniok, S. Paul, M. Capron, and F. Dumeignil, *ChemSusChem.* 2, 719 (2009).
9. E. H. Xie, Q. L. Zhang, and K. T. Chuang, *Appl. Catal. A: Gen.* 220, 215 (2001).
10. C.-J. Jia, Y. Liu, W. Schmidt, A.-H. Lu, and F. Sch th, *J. Catal.* 269, 71 (2010).
11. S.-H. Chai, H.-P. Wang, Y. Liang, and B.-Q. Xu, *J. Catal.* 250, 342 (2007).
12. A. Ulgen and W. Hoelderich, *Catal. Lett.* 131, 122 (2009).
13. I. V. Kozhevnikov, *Chem. Rev.* 98, 171 (1998).
14. T. Okuhara, N. Mizuno, and M. Misono, *Adv. Catal.* 41, 113 (1996).
15. P. M. Sreekanth and P. G. Smirniotis, *Catal. Lett.* 122, 37 (2008).
16. J. Hong, W. Chu, M. Chen, X. Wang, and T. Zhang, *Catal. Commun.* 8, 593 (2007).
17. J.-Y. Zheng, J.-B. Pang, K.-Y. Qiu, and Y. Wei, *Micropor. Mesopor. Mater.* 49, 189 (2001).
18. K. M. Reddy, C. V. G. Reddy, and S. V. Manorama, *J. Solid State Chem.* 158, 180 (2001).
19. J. C. Edwards, C. Y. Thiel, B. Benac, and J. F. Knifton, *Catal. Lett.* 51, 77 (1998).
20. J. E. Sunstrom IV, W. R. Moser, and B. Marshik-Guerts, *Chem. Mater.* 8, 2061 (1996).
21. F. Jin and Y. Li, *Catal. Today* 145, 101 (2009).
22. C. A. Emeis, *J. Catal.* 141, 347 (1993).
23. G. S. Kumar, M. Vishnuvarthan, M. Palanichamy, and V. Murugesan, *J. Mol. Catal. A: Chem.* 260, 49 (2006).
24. B. C. Gagea, Y. Lorgouilloux, Y. Altintas, P. A. Jacobs, and J. A. Martens, *J. Catal.* 265, 99 (2009).
25. J. Barrault, J.-M. Clacens, and Y. Pouilloux, *Top. Catal.* 27, 137 (2004).
26. W. Suprun, M. Lutecki, T. Haber, and H. Papp, *J. Mol. Catal. A: Chem.* 309, 71 (2009).
27. M. Massa, A. Andersson, E. Finocchio, G. Busca, F. Lenrick, and L. R. Wallenberg, *J. Catal.* 297, 93 (2013).
28. A. Alhanash, E. F. Kozhevnikova, and I. V. Kozhevnikov, *Appl. Catal. A: Gen.* 378, 11 (2010).

Received: 9 July 2015. Accepted: 17 February 2016.